Finite-Size Effects on Liquid-Solid Phase Coexistence and the Estimation of Crystal Nucleation Barriers

Antonia Statt,[1,2,*] Peter Virnau,[1] and Kurt Binder[1]
[1]Institut für Physik, Johannes Gutenberg-Universität Mainz, Staudinger Weg 9, 55128 Mainz, Germany
[2]Graduate School of Excellence Materials Science in Mainz, Staudinger Weg 9, 55128 Mainz, Germany
(Received 15 October 2014; published 13 January 2015)

A fluid in equilibrium in a finite volume V with particle number N at a density $\rho = N/V$ exceeding the onset density ρ_f of freezing may exhibit phase coexistence between a crystalline nucleus and surrounding fluid. Using a method suitable for the estimation of the chemical potential of dense fluids, we obtain the excess free energy due to the surface of the crystalline nucleus. There is neither a need to precisely locate the interface nor to compute the (anisotropic) interfacial tension. As a test case, a soft version of the Asakura-Oosawa model for colloid-polymer mixtures is treated. While our analysis is appropriate for crystal nuclei of arbitrary shape, we find the nucleation barrier to be compatible with a spherical shape and consistent with classical nucleation theory.

DOI: 10.1103/PhysRevLett.114.026101 PACS numbers: 68.03.Cd, 64.60.Q-, 68.08.-p

The nucleation of crystals from fluid phases and their subsequent growth is one of the most important phase transformations in nature [1–3]; applications range from ice crystal formation in the atmosphere, to metallurgy, nanomaterials, protein crystallization, etc. Despite its overwhelming importance, crystal nucleation remains poorly understood.

For the nucleation of a liquid drop from supersaturated vapor, the average nucleus shape is clearly spherical. Only the curvature dependence of the interfacial tension [4–9] presents a stumbling block for the prediction of nucleation barriers. Unlike interfaces between fluid phases, the crystal-fluid interface tension $\gamma(\vec{n})$ depends on the orientation of the interface normal $\vec{n}$ relative to the crystal lattice axes [10–12]. For isotropic γ, the nucleus is a sphere of radius R (volume $V = 4\pi R^3/3$) and its surface excess free energy is $F_{\rm surf} = 4\pi R^2\gamma = A_{\rm iso}\gamma V^{2/3}$, with $A_{\rm iso} = (36\pi)^{1/3}$. For crystals, the term $A_{\rm iso}\gamma$ is replaced by a complicated expression

$$F_{\rm surf}(V) = \int_{A_W} \gamma(\vec{n}) d\vec{s} V^{2/3} \equiv A_W \bar{\gamma} V^{2/3}. \quad (1)$$

Here, A_W is the surface area of a unit volume whose shape is derivable from $\gamma(\vec{n})$ via the Wulff construction [10–12], and the average interface tension $\bar{\gamma}$ is defined as $\bar{\gamma} = A_W^{-1} \int \gamma(\vec{n}) d\vec{s}$.

In the classical nucleation theory [1–3], the formation free energy of a nucleus is written in terms of volume and surface terms as

$$\Delta F = -(p_c - p_l)V + F_{\rm surf}(V). \quad (2)$$

Here, p_c is the pressure in the crystal nucleus and p_l in the (metastable) liquid phase surrounding it. In the thermodynamic limit, the configuration with one nucleus on top of the free-energy barrier in the metastable phase is a saddle point in configuration space. The condition for (unstable) equilibrium $\partial(\Delta F)/\partial V = 0$ then yields the critical nucleus volume V^* and barrier ΔF^*,

$$V^* = \left[\frac{2A_W\bar{\gamma}}{3(p_c - p_l)}\right]^3, \quad \Delta F^* = \frac{1}{3}A_W\bar{\gamma}V^{*2/3} = \frac{1}{2}(p_c - p_l)V^*. \quad (3)$$

Even if V^* is large enough so that correction terms to Eq. (2) can be neglected, the application of Eq. (3) is difficult due to lack of knowledge on A_W and $\bar{\gamma}$. This lack of knowledge has hampered the comparison of observed nucleation rates [13–16] (and the barriers extracted from them) and simulations [17–20] where ΔF^* was estimated directly by biased sampling methods. These comparisons were made for suspensions of (hard spherelike) colloidal particles; the large size of the colloids has the advantage of allowing direct microscopic observations of crystal-liquid interfaces [21] and nucleation events [22,23]. Since kinetic processes for colloids are many orders of magnitude slower than those for small molecules, colloids are model systems for the study of the liquid-solid transition [24,25] and well suited to separate nucleation from the subsequent crystal growth.

However, to elucidate the persisting discrepancies between simulations and experiments, one needs to know more about the theoretical nucleation barriers: How large must V^* be so that Eq. (3) is a good approximation? What is the physical origin of corrections to ΔF^* [Eq. (3)] and their magnitude? Is it legitimate to assume a spherical shape of the nucleus, despite its crystalline structure? And so on. Understanding the general conditions under which the classical description [Eqs. (2), (3)] holds will be useful to understand liquid-solid transitions in condensed matter in general.

In the present Letter, we address these issues and show how both V^* and ΔF^* can be obtained, considering the equilibrium of the system at fixed finite particle number N in a finite simulation box $V_{\rm box}$. For a suitable range of density $\rho = N/V_{\rm box}$, the equilibrium between the crystalline nucleus and surrounding fluid is perfectly stable. We explain how both V^* and $p_c - p_l$ can be estimated directly and accurately. Using then $\Delta F^* = (p_c - p_l)V^*/2$ [Eq. (3)], the need of dealing with $\gamma(\bar{n})$ and the use of Eq. (1) is bypassed. So we do not need to assume anything on the shape of the nucleus.

Thus, the central idea of the present work is to explore the deviations from phase coexistence in the thermodynamic limit (where the chemical potential $\mu = \mu_{\rm coex}$ and the pressure $p = p_{\rm coex}$ for all densities from the onset density of freezing ρ_f to the onset density of melting ρ_m) caused by finite size. Thus, the part of the isotherm in Fig. 1 corresponding to the homogeneous fluid for finite volume $V_{\rm box}$ exceeds ρ_f and continues up to the "droplet evaporation condensation transition" [26] at ρ_1, where for the first time a crystalline droplet in the system becomes stable. Note that this transition is a sharp phenomenon only when $V_{\rm box} \to \infty$ (and then $\rho_1 \to \rho_f$, consistent with the lever rule [27]). At a second special density ρ_2, the "droplet" changes its shape from compact to cylindrical (stabilized by the periodic boundary conditions). At about $\rho = \rho_3$ a slab configuration, separated from the fluid by two planar interfaces, appears (Fig. 1). In this region, $\mu = \mu_{\rm coex}$ and

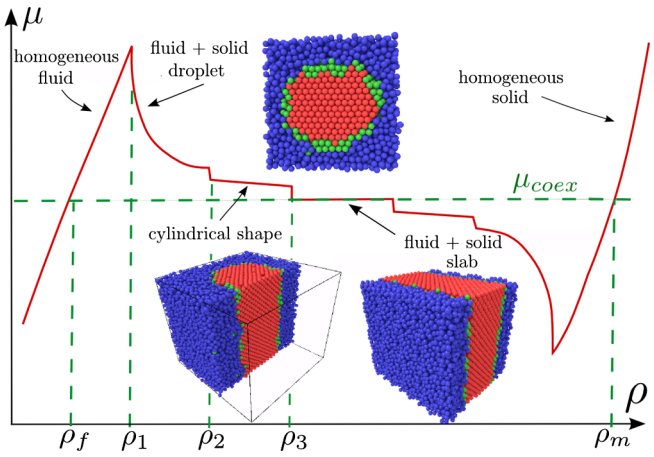

FIG. 1 (color online). Schematic plot of the chemical potential μ vs density ρ for a system undergoing a liquid-solid transition in a finite box volume $V_{\rm box}$ with periodic boundary conditions. (A plot of pressure p vs ρ would qualitatively look just the same). Because of interfacial effects, non-negligible in finite systems, the isotherm deviates from $p = p_{\rm coex}$ in the two-phase coexistence region, $\rho_f < \rho < \rho_m$. The features in the curve (kinks in reality are rounded due to fluctuations) are due to transitions between the different states shown in the figure via snapshots of the simulated generalized Asakura-Oosawa model. Only the part where the solid phase is the minority phase is discussed. For further explanations, see the text.

$p = p_{\rm coex}$ holds true also in the finite system, if the linear dimensions in the directions parallel to the planar interfaces are chosen such that the crystal (at density ρ_m) is commensurate without any distortion. The analogous behavior for vapor to liquid transitions is well studied [9,28–30]. Here, we show that the descending part of the $p(\rho)$ and $\mu(\rho)$ isotherms can be used to extract information on $F_{\rm surf}$, V^* and ΔF^* for the liquid-solid transition as well.

In the snapshots, the particles in the fluid region are shown in blue and in the crystal are shown in red, using the averaged Steinhardt local bond order parameters [31,32] to distinguish the character of the phases (see Ref. [32] for definitions and implementation details). Particles in the interfacial region, for which this classification yielded ambiguous results, are shown in green color. The face-centered cubic (fcc) packing of the crystal is clearly seen, and the cross section through the droplet also suggests that the shape may be nonspherical.

The model of our simulations qualitatively describes colloid-polymer mixtures [33–36]. In the Asakura-Oosawa (AO) model [33], colloids are described by hard spheres of diameter σ_c and polymers as soft spheres (which may overlap each other without energy cost) of diameter σ_p. Of course, the mutual overlap of colloids and polymers is also strictly forbidden. Polymers create the (entropic) depletion attraction between colloids [33]; varying the size ratio $q = \sigma_p/\sigma_c$ and the polymer density, one can tune the phase diagram [34–36] and interfacial properties [37,38]. A useful feature of this model occurs for $q < q^* = 0.154$ [35,39]; then one can integrate out the polymer degrees of freedom exactly, and one is left with an effective pairwise potential, which is attractive in the range of $\sigma_c < r < \sigma_c + \sigma_p$ (and zero for $r > \sigma_c + \sigma_p$), but infinitely repulsive for $r < \sigma_c$. The strength of the potential of this "effective" (Eff) AO model is controlled by the fugacity z_p of the polymers [39] (Fig. 2, inset).

However, it is computationally more convenient to replace the Eff AO model by a similar but continuous potential, the soft Eff AO model [39] (Fig. 2, inset). For this model, the pressure (in the fluid phase) is straightforwardly obtained in the simulation from the Virial expression [39,40], while for the Eff AO model due to the discontinuity at $r = \sigma_c$ this is very cumbersome [38]. Figure 2 shows that the variation of p with η is very similar for both potentials. Since real colloids never are described by hard spheres precisely [41], nor are polymers precisely modeled by ideal soft spheres [42], a quantitatively accurate modeling of real systems cannot be attempted anyway. The soft Eff AO model is proposed here as a coarse-grained qualitative model of colloid-polymer mixtures, which is practically useful in a simulation context.

With the use of the Virial expression, the pressure p_l of the liquid in the region surrounding the crystal nucleus in Fig. 1 (far from the interfacial region) can be readily measured, but obtaining p_c inside the nucleus for small

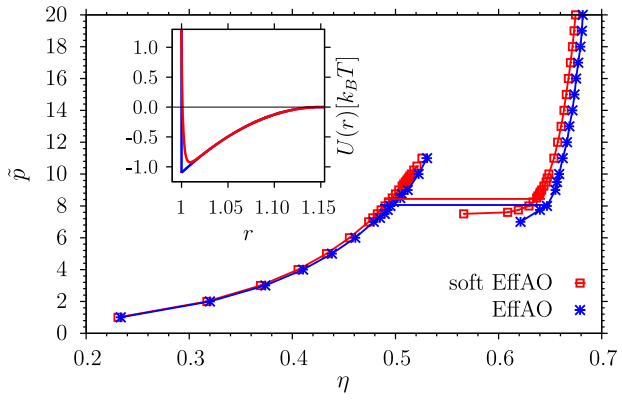

FIG. 2 (color online). Normalized pressure $\tilde{p} = p\sigma_c^3/k_BT$ plotted vs packing fraction $\eta \equiv \rho\pi\sigma_c^3/6$ of the colloids, for the Eff AO model (asterisks) and its soft version (soft Eff AO, squares). Curves are a guide to the eye only. These data were obtained from simulations of homogeneous liquid and solid (fcc) phases, while the pressure where two-phase coexistence occurs was found from the "interface velocity method" [37], namely, $\tilde{p} = 8.44 \pm 0.04$ (soft Eff AO) and $\tilde{p} = 8.06 \pm 0.06$ (Eff AO). The coexistence packing fractions are $\eta_f = 0.495(1)$ and $\eta_m = 0.636(1)$ for the soft Eff AO case. The inset compares the potentials of the Eff AO (which is singular at $r = \sigma_c = 1$) and soft Eff AO models.

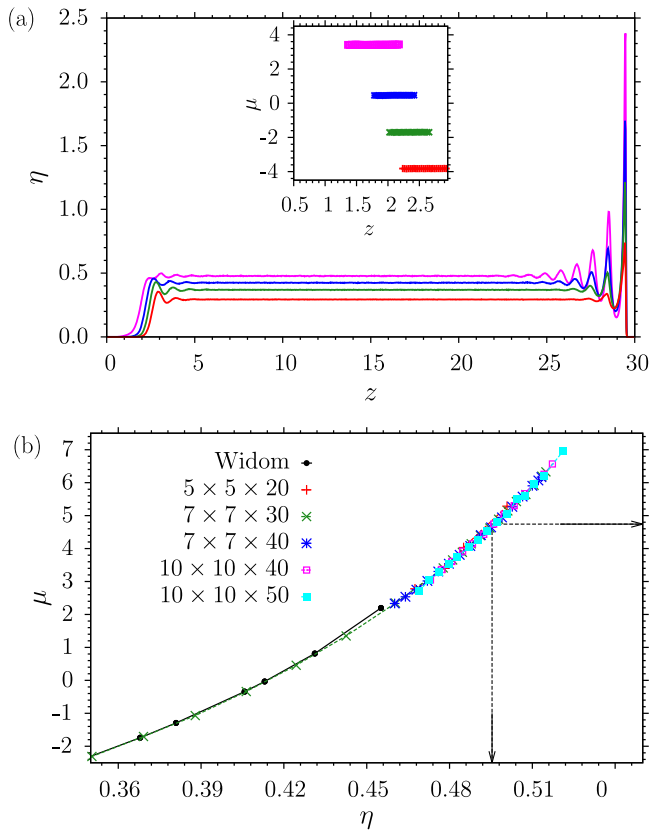

FIG. 3 (color online). (a) Illustration of the method to compute the chemical potential of a very dense fluid, using an $L \times L \times L_z$ slab geometry, with a soft wall at $z = 0$ and a hard wall at $z = L_z = 30$ (lengths being measured in units of σ_c, $L = 7$, and four choices of N are used, $N = 750$, 950, 1100 and 1250, respectively). Inset shows μ in units of k_BT as a function of z, for the four choices shown, over the regions of z where particle insertion works. (b) Chemical potential μ (in units of k_BT) plotted vs η, for different choices of L and L_z, as indicated, to show that finite-size effects are negligible. The data labeled by "Widom" at not so large η values are obtained by the standard particle insertion method for homogeneous bulk systems. Arrows on abscissa and ordinate indicate η_f and $\mu_c(p_{\rm coex})/k_BT$, respectively.

nuclei is not reliably possible. It is necessary to base the analysis of the two-phase equilibrium in $V_{\rm box}$ on the chemical potential μ, because μ is strictly constant in equilibrium also in a spatially inhomogeneous situation. But the standard particle insertion method [40,43] does not work at high packing fractions η near η_m. Thus, we have extended an approach [44] to sample the chemical potential of a dense fluid by studying a system where walls are present, using a soft wall that reduces the density suitably such that particle insertion works there (Fig. 3). Of course, it is important to choose L_z large enough so that outside of the range of z, for which the walls affect the density profile, a constant density is actually reached. Figure 3 demonstrates that in this way the chemical potential can be obtained accurately even for $\eta > \eta_f$. The pressure p [computed in the region where $\eta(z) = \eta_{\rm bulk} = \text{constant}$] agrees with the corresponding bulk data of Fig. 2.

Now we exploit the fact that μ is constant throughout the system also when a crystalline nucleus is present (Fig. 1): the chemical potential in the fluid $\mu_f(p_l)$ equals that of the crystal nucleus $\mu_c(p_c)$. From $\mu_c(p_{\rm coex}) = \mu_l(p_{\rm coex}) = \mu_{\rm coex}$ we readily find, using the expansions

$$\mu_c(p_c) \approx \mu_{\rm coex} + \frac{\pi}{6}\frac{1}{\eta_m}(p_c - p_{\rm coex}), \tag{4}$$

$$\mu_l(p_l) \approx \mu_{\rm coex} + \frac{\pi}{6}\frac{1}{\eta_f}(p_l - p_{\rm coex}), \tag{5}$$

that $(p_c - p_{\rm coex})\eta_f = (p_l - p_{\rm coex})\eta_m$. Since we have recorded both functions $\mu_l(\eta)$ and $p_l(\eta)$, we also know $\mu_l(p_l)$ and, hence, can verify that the data indeed fall in the regime where the linear expansion of Eq. (5) holds. Finding $\mu_c(p_c)$ via thermodynamic integration [using $\mu_c(p_{\rm coex}) = \mu_l(p_{\rm coex})$ as the starting point], we have verified that Eq. (4) also introduces only negligible errors.

The two-phase equilibrium of a crystalline droplet surrounded by fluid has been studied for three system sizes, keeping the number of colloids in the simulation box fixed (at $N = 6000$, 8000, and 10 000, respectively) and varying $V_{\rm box}$ and hence $\rho = N/V_{\rm box}$. In thermal equilibrium, we then have a finite-size variant of the lever rule

$$\eta V_{\rm box} = \eta_l(p_l)(V_{\rm box} - V^*) + \eta_c(p_c)V^*. \tag{6}$$

While for $V_{\rm box} \to \infty$ we would have $p_l = p_c = p_{\rm coex}$ and $\eta_c(p_{\rm coex}) = \eta_m$, in the finite system p_l, p_c and the

corresponding packing fractions differ from their coexistence values. Initializing the simulation by putting a crystal of about the right volume V^* and about the right choice for $\eta_c(p_c)$ in the box, after a long period of equilibration we measure both p_l and $\eta_l(p_l)$ in the fluid region (far from the crystal) and verify [from the data of the bulk simulation, Fig. 3(b)] that equilibrium has been reached. Since we know also the chemical potential [$\mu_c(p_c) = \mu_l(p_l)$ is constant], we can obtain p_c and also $\eta_c(p_c)$, and hence, Eq. (6) determines V^* unambiguously.

Figure 4 shows the data for $\Delta p = p_l - p_{\rm coex}$ vs η. Actually, when we use the chemical potential $\mu_l(p_l)$ from Fig. 3(b) and obtain Δp from Eq. (5), the data are precisely reproduced, which is just a consistency check. From simulations determining γ for interfaces parallel to 111, 110 and 100 planes [45], it is found that $\gamma(\vec{n})$ depends only very weakly on $\vec{n}$. For comparison with classical nucleation theory, we neglect the dependence on $\vec{n}$ and take $\gamma \approx \gamma_{111} \approx \gamma(\vec{n}) = 1.013$ [45]. Assuming a spherical shape $V^* = 4\pi R^{*3}/3$, we find $\Delta p = (2\gamma/R^*)/(\eta_m/\eta_f - 1)$. Using the observed values of V^* one then obtains a prediction for the curves $\Delta p(\eta)$. We find that these predicted curves fall slightly below the actual observed data. They can be brought in good agreement if they are rescaled by a constant factor of $c = 1.07$. This small enhancement can be due to the ratio $A/A_{\rm iso}$ or errors in the estimation of $\gamma(\vec{n})$. Unexpectedly, we hence find that for our model of colloid-polymer mixtures the assumption of a spherical nucleus shape works rather well, but it would not be needed to predict the nucleation barrier. With the use of Eq. (2), knowledge of $p_c - p_l$ and V^* suffices to predict ΔF^*. One can expect, however, that significant derivations from spherical nucleus shape will appear for large η_p^r in our model, where the fluid is a vaporlike phase, and $\gamma(\vec{n})$ will depend more strongly on $\vec{n}$. Gratifyingly, Fig. 4(b) shows that the three choices for N superimpose to a common curve, so in the shown regime finite-size effects essentially are negligible.

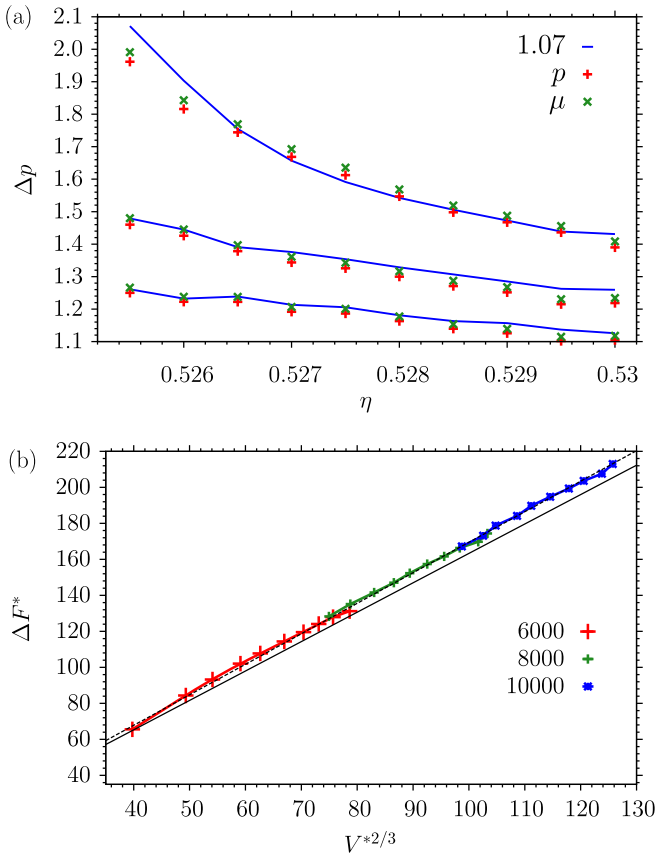

FIG. 4 (color online). (a) Pressure difference $\Delta p = p_l - p_{\rm coex}$ between the pressure p_l in a fluid surrounding a crystal nucleus of finite size and the coexistence pressure, plotted vs the average packing fraction η in the simulation box, for particle number $N = 6000$, 8000, and 10 000 (symbols, from bottom to top). Curves show the formula $\Delta p = (2\gamma/R^*)c/(\eta_m/\eta_f - 1)$ with $c = 1.07$, extracting R^* from the assumption of a spherical nucleus ($V^* = 4\pi R^{*3}/3$) and taking $\gamma \approx \tilde{\gamma}_{111} \approx 1.013$ [45]. (b) ΔF^* computed from p_l, p_c and V^* [using Eqs. (2), (5), and (6)] plotted vs $V^{*2/3}$; straight line is Eq. (3) with $A = A_{\rm iso}$ and $\tilde{\gamma} = \gamma_{111}$. The dotted line is a fit illustrating $\Delta F^* \propto V^{*2/3}$.

In summary, we have shown that for the liquid-solid transition a description of nucleation barriers in terms of the classical nucleation theory holds, at variance with studies of nucleation with hard spherelike colloids [13–20,46]. However, we feel the latter studies are inconclusive, due to their use of too large η_l ($0.53 < \eta_l < 0.57$) where the slowing down due to the kinetic prefactor of the nucleation rate matters [47]. While the range of ΔF^* in Fig. 4(b) corresponds to $\eta_l/\eta_f - 1 \leq 0.06$, the range of the experiments in Fig. 4(b) would correspond to $5 < \Delta F^* < 10$ only.

By an analysis of finite-size effects on phase coexistence, both V^*, p_l, p_c and the chemical potential for this stable two-phase coexistence in a finite simulation box can be reliably estimated. The numerical results also clearly show that in the regime where $\Delta F^* \geq 80$ the relation $\Delta F^* \propto V^{*2/3}$ holds precisely, as visible from the fit in Fig. 4(b); thus, we have verified that classical theory of homogeneous nucleation for crystals is accurate, in this regime of barriers, provided one takes into account that the nucleus shape is in general nonspherical. However, since the two straight lines in Fig. 4(b) almost coincide, the spherical approximation is shown here to be almost perfect. Since crystal faces in contact with a dense fluid are frequently atomically rough, the spherical approximation is expected to be quite good generally, in particular for somewhat smaller nuclei, for which the nucleation rates also would be larger.

This research was supported by the Deutsche Forschungsgemeinschaft (Grant No. VI237/4-3). We thank the Höchstleistungsrechenzentrum Stuttgart (HLRS) and the Zentrum für Datenverarbeitung Mainz for generous grants of computing time at the HERMIT and MOGON supercomputers.

*Corresponding author.
statt@uni-mainz.de

[1] *Nucleation*, edited by A. C. Zettlemoyer (M. Dekker, New York, 1969).
[2] D. Kashchiev, *Nucleation: Basic Theory with Applications* (Butterworth-Heinemann, Oxford, 2000).
[3] K. F. Kelton and A. L. Greer, *Nucleation* (Pergamon, Oxford, 2009).
[4] R. C. Tolman, J. Chem. Phys. **17**, 333 (1949).
[5] M. A. Anisimov, Phys. Rev. Lett. **98**, 035702 (2007).
[6] B. J. Block, S. K. Das, M. Oettel, P. Virnau, and K. Binder, J. Chem. Phys. **133**, 154702 (2010).
[7] S. K. Das and K. Binder, Phys. Rev. Lett. **107**, 235702 (2011).
[8] A. Tröster and K. Binder, Phys. Rev. Lett. **107**, 265701 (2011).
[9] A. Tröster, M. Oettel, B. J. Block, P. Virnau, and K. Binder, J. Chem. Phys. **136**, 064709 (2012).
[10] G. Wulff, Z. Kristallogr. Mineral **34**, 449 (1901).
[11] C. Herring, Phys. Rev. **82**, 87 (1951).
[12] C. Rottmann and M. Wortis, Phys. Rep. **103**, 59 (1984).
[13] K. Schätzel and B. J. Ackerson, Phys. Rev. E **48**, 3766 (1993).
[14] Y. M. He, B. J. Ackerson, W. van Megen, S. M. Underwood, and K. Schätzel, Phys. Rev. E **54**, 5286 (1996).
[15] J. L. Harland and W. van Megen, Phys. Rev. E **55**, 3054 (1997).
[16] C. Sinn, A. Heymann, A. Stipp, and T. Palberg, Prog. Colloid Polym. Sci. **118**, 266 (2001).
[17] S. Auer and D. Frenkel, Nature (London) **409**, 1020 (2001).
[18] L. Filion, M. Hermes, R. Ni, and M. Dijkstra, J. Chem. Phys. **133**, 244115 (2010).
[19] T. Schilling, S. Dorosz, H. J. Schöpe, and G. Opletal, J. Phys. Condens. Matter **23**, 194120 (2011).
[20] L. Filion, R. Ni, D. Frenkel, and M. Dijkstra, J. Chem. Phys. **134**, 134901 (2011).
[21] J. Hernandez-Guzman and E. R. Weeks, Proc. Natl. Acad. Sci. U.S.A. **106**, 15198 (2009).
[22] U. Gasser, E. R. Weeks, A. Schofield, P. N. Pusey, and D. A. Weitz, Science **292**, 258 (2001).
[23] Z. Wang, F. Wang, Y. Peng, Z. Zheng, and Y. Han, Science **338**, 87 (2012).
[24] P. N. Pusey and W. van Megen, Nature (London) **320**, 340 (1986).
[25] D. M. Herlach, I. Klassen, P. Wette, and D. Holland-Moritz, J. Phys. Condens. Matter **22**, 153101 (2010).
[26] K. Binder, Physica (Amsterdam) **319A**, 99 (2003).
[27] L. D. Landau and E. M. Lifshitz, *Statistical Physics*, 3rd ed. (Pergamon, Oxford, 1980).
[28] L. G. MacDowell, P. Virnau, M. Müller, and K. Binder, J. Chem. Phys. **120**, 5293 (2004).
[29] L. G. MacDowell, V. K. Shen, and J. R. Errington, J. Chem. Phys. **125**, 034705 (2006).
[30] K. Binder, B. J. Block, P. Virnau, and A. Troester, Am. J. Phys. **80**, 1099 (2012).
[31] P. J. Steinhardt, D. R. Nelson, and M. Ronchetti, Phys. Rev. B **28**, 784 (1983).
[32] W. Lechner and C. Dellago, J. Chem. Phys. **129**, 114707 (2008).
[33] S. Asakura and F. Oosawa, J. Polym. Sci. **33**, 183 (1958).
[34] H. N. W. Lekkerkerker, W. C. K. Poon, P. N. Pusey, A. Stroobants, and P. B. Warren, Europhys. Lett. **20**, 559 (1992).
[35] M. Dijkstra, R. van Roij, and R. Evans, Phys. Rev. E **59**, 5744 (1999).
[36] W. C. K. Poon, J. Phys. Condens. Matter **14**, R859 (2002).
[37] T. Zykova-Timan, J. Horbach, and K. Binder, J. Chem. Phys. **133**, 014705 (2010).
[38] D. Deb, A. Winkler, P. Virnau, and K. Binder, J. Chem. Phys. **136**, 134710 (2012).
[39] The Eff AO potential shown in Fig. 2 is $U(r) = \infty$ for $\sigma_c < r$ and $U(r) = -\eta_p^r \left(\frac{1+q}{q}\right)^3 \left[1 - \frac{3r}{2\sigma_c(1+q)} + \left(\frac{r}{2\sigma_c(1+q)}\right)^3\right]$ for $\sigma_c < r < \sigma_c + \sigma_p$ and for $r > \sigma_c + \sigma_p U(r) = 0$. Here (consistent with Ref. [37]), $q = 0.15$, $\eta_p^r = 0.1$ is chosen. The soft Eff AO model replaces the hard core interaction part by adding a polynomial $U_{\mathrm{rep}}(r) = 4\left[\left(\frac{b\sigma_c}{r - e\sigma_c}\right)^{12} + \left(\frac{b\sigma_c}{r - e\sigma_c}\right)^{6} - \left(\frac{b\sigma_c}{\sigma_c + q - e\sigma_c}\right)^{12} - \left(\frac{b\sigma_c}{\sigma_c + q - e\sigma_c}\right)^{6}\right]$ to the potential with constants $e = 0.98857$ and $b = 0.01$.
[40] M. P. Allen and D. J. Tildesley, *Computer Simulation of Liquids* (Clarendon Press, Oxford, 1989).
[41] C. P. Royall, W. C. K. Poon, and E. R. Weeks, Soft Matter **9**, 17 (2013).
[42] P. G. Bolhuis, A. A. Louis, and J. P. Hansen, Phys. Rev. Lett. **89**, 128302 (2002).
[43] B. Widom, J. Chem. Phys. **39**, 2808 (1963).
[44] J. G. Powles, B. Holtz, and W. A. B. Evans, J. Chem. Phys. **101**, 7804 (1994).
[45] F. Schmitz, Dissertation, Johannes Gutenberg Universität Mainz (unpublished).
[46] T. Palberg, J. Phys. Condens. Matter **26**, 333101 (2014).
[47] M. Radu and T. Schilling, Europhys. Lett. **105**, 26001 (2014).